Image Fusion Algorithm Based on Spatial Frequency-Motivated Pulse Coupled Neural Networks in Nonsubsampled Contourlet Transform Domain

QU Xiao-Bo[1]   YAN Jing-Wen[1, 2]   XIAO Hong-Zhi[2]   ZHU Zi-Qian[3]

Abstract   Nonsubsampled contourlet transform (NSCT) provides flexible multiresolution, anisotropy, and directional expansion for images. Compared with the original contourlet transform, it is shift-invariant and can overcome the pseudo-Gibbs phenomena around singularities. Pulse coupled neural networks (PCNN) is a visual cortex-inspired neural network and characterized by the global coupling and pulse synchronization of neurons. It has been proven suitable for image processing and successfully employed in image fusion. In this paper, NSCT is associated with PCNN and used in image fusion to make full use of the characteristics of them. Spatial frequency in NSCT domain is input to motivate PCNN and coefficients in NSCT domain with large firing times are selected as coefficients of the fused image. Experimental results demonstrate that the proposed algorithm outperforms typical wavelet-based, contourlet-based, PCNN-based, and contourlet-PCNN-based fusion algorithms in terms of objective criteria and visual appearance.

Key words   Contourlet, pulse coupled neural networks (PCNN), wavelet, image fusion, multiscale transform

Image fusion is the combination of two or more different images to form a new image by using a certain algorithm[1]. The combination of sensory data from multiple sensors can provide reliable and accurate information. It forms a rapidly developing research area in remote sensing, medical image processing, and computer vision[1−2]. Most of these approaches are based on combining the multiscale decompositions (MSD) of the source images. MSD-based fusion schemes provide much better performance than the simple methods studied previously[2]. These methods decompose the source images into high-frequency and low-frequency subbands. Detailed and coarse features remain in the two types of subbands, respectively. Two core questions of MSD-based fusion algorithms are which MSD method should be used and how to combine coefficients in subbands.

For the first question, the discrete wavelet transform (DWT) becomes the most popular MSD method in image fusion because of joint information represented at the spatial-spectral domain. However, wavelet has its own limits. It is expensive for wavelet to represent sharp image transitions such as edges[3]. Furthermore, wavelet will not "see" the smoothness along the contours and separable wavelets can only capture limited directional information[4]. Thus, new MSD transforms are introduced in image fusion (i.e., bandelet[5], curvelet[6], contourlet[7−9], etc.) to overcome the limits of wavelet. Contourlet was recently pioneered by Do[4]. Compared with wavelet, it provides different and flexible number of directions at each scale and can capture the intrinsic geometrical structure. However, the original contourlet[4] lacks shift-invariance and causes pseudo-Gibbs phenomena around singularities. Nonsubsampled contourlet transform (NSCT)[10], as a fully shift-invariant form of contourlet, leads to better frequency selectivity and regularity. Thus, NSCT is used as the MSD method in this paper.

For the second question, the typical fusion algorithms are based on the activity-level measurement. Coefficients in MSD domain with high activity-level are selected to compose the fused image[2]. In this paper, we present a bio-inspired activity-level measure based on pulse coupled neural networks (PCNN). PCNN is a novel biological neural network developed by Eckhorn in 1990 and based on the experimental observations of synchronous pulse bursts in cat and monkey visual cortex[11−12]. It is characterized by the global coupling and pulse synchronization of neurons. These characteristics benefit image fusion which makes use of local image information. PCNN has been successfully used in image fusion[9, 13−17]. Pixels in subbands images in MSD domain (named coefficients and simplified into coef in figures and tables in this paper) or pixels in spatial domain with greater firing times are considered in high activity-level. However, in these PCNN-based algorithms, the value of single pixel in spatial or MSD domain is used to motivate one neuron. In fact, humans are often sensitive to edges, directional features, etc. So, a pure use of single pixels is not enough. In this paper, spatial frequency, which stands for gradient energy in NSCT domain, is used to motivate PCNN neurons for the first time.

For simplicity, we term the proposed algorithm as spatial frequency-motivated PCNN in NSCT domain, NSCT-SF-PCNN for short. In this algorithm, the flexible multiresolution, anisotropy, and directional expansion for images of NSCT are associated with global coupling and pulse synchronization characteristic of PCNN. We tend to take PCNN for nonlinear filter to select coefficients in image fusion. Experimental results demonstrate that the proposed algorithm outperforms typical wavelet-based, contourlet-based, NSCT-based, PCNN-based, and contourlet-PCNN-based fusion algorithms in terms of objective criteria and visual appearance.

1 Contourlet and PCNN in image fusion

1.1 Contourlet in image fusion

Contourlet is proposed by Do to obtain a sparse expansion for smooth contours[4], which overcomes the limitation of wavelet in representing the contours by using square-shaped brush strokes and many fine "dots". In the

contourlet, the Laplacian pyramid (LP) is first used to capture the point discontinuities and then followed by a directional filter bank (DFB) to link point discontinuities into linear structures. The number of direction decomposition at each level can be different, which is much more flexible than the three directions in wavelet. Unfortunately, in the original contourlet[4], downsamplers and upsamplers are presented in both LP and DFB as shown in Fig. 1 (a). Thus, it is shift-invariant and causes pseudo-Gibbs phenomena around singularities. NSCT is proposed by Da[10], which aims to overcome this disadvantage. Fig. 1 (b) shows the decomposition framework of NSCT. Nonsubsampled pyramid structure (NPS) and nonsubsampled DFB are used in NSCT. The NPS is achieved by using two-channel nonsubsampled 2-D filter banks. The DFB is achieved by switching off the downsamplers/upsamplers in each two-channel filter bank in the DFB tree structure and upsampling the filters accordingly. As a result, NSCT yields better frequency selectivity, regularity, and shift-invariance.

In the contourlet-based image fusion algorithms[7−9], contourlet or NSCT is used as the MSD method. As absolute value measure in high-frequency and average rule in low-frequency subbands are the typical activity level measure in other MSD-based fusion algorithms, activity-level are measured on the coefficients of subbands in contourlet domain. Coefficients with high activity-level are selected as the coefficients of fused subbands and an inverse contourlet is performed to reconstruct the fused image. The framework of contourlet-based algorithms is shown in Fig. 2.

1.2   PCNN in image fusion

PCNN is a feedback network and each PCNN neuron consists of three parts: the receptive field, the modulation field, and the pulse generator[12]. In image processing, PCNN is a single layer pulse coupled neural cells with a two-dimensional connection[13] as shown in Fig. 3.

In the existing PCNN-based fusion algorithms [9, 14−17], pixels in spatial or MSD domain are input to PCNN, and there exists a one-to-one correspondence between the pixels and the neurons. Each neuron is connected with neighboring neurons in the linking range. The output of each neuron results in two states, namely firing and non-firing. Then, the sum of neuron firing times will generate a firing map whose size is equal to the images in spatial or MSD domain and the value of each pixel in firing map is equal to neuron firing times. We summarize these algorithms as Fig. 4. The value of pixels in spatial or MSD domain is considered as the original image information in the existing algorithms. However, a pure use of pixels is not effective enough because humans are often sensitive to edges and directional features. We believe it will be more reasonable to employ features, rather than value of pixels, to motivate PCNN.

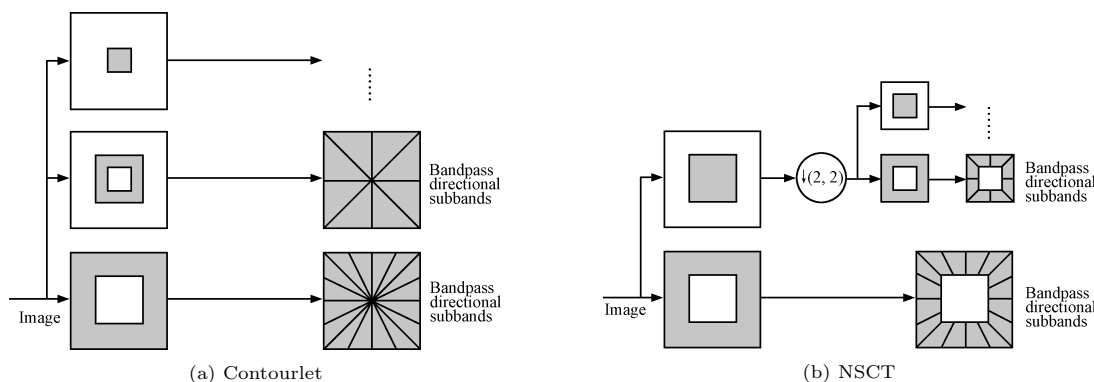(a) Contourlet   (b) NSCT

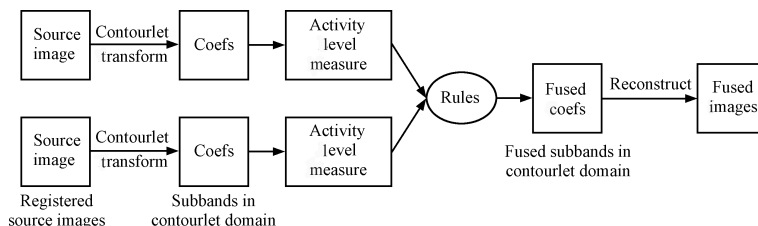Fig. 1   Decomposition framework of contourlet and NSCT

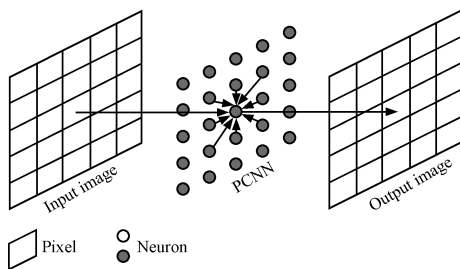Fig. 2   Schematic diagram of contourlet-based fusion algorithm
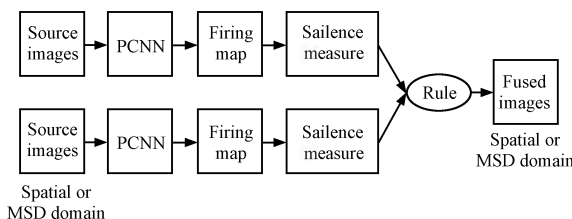

Fig. 3   Connection model of PCNN neuron

Fig. 4   Schematic diagram of existed PCNN-based fusion algorithms

2 Image fusion algorithm based on NSCT-SF-PCNN

2.1 NSCT-SF-PCNN

For the first time, Fang successfully used PCNN in contourlet domain for visible and infrared image fusion[9]. However, the contourlet used in [9] is the original form and lacks shift-invariance. In addition, single coefficient is used to motivate PCNN directly. In fact, humans are often sensitive to features, e.g. edges. So, a pure use of value of single coefficient is not enough.

In this paper, NSCT is used as the MSD method to provide a better representation of the contours than wavelet and it overcomes pseudo-Gibbs phenomena around singularities of contourlet. What is more, instead of using PCNN in contourlet domain directly, spatial frequency (SF)[18] in contourlet domain is considered as the gradient features of images and we use SF to motivate PCNN instead. For simplicity, we term the proposed algorithm as NSCT-SF-PCNN.

Let $I_{i,j}^{l,k}$ denote the coefficients located at (i,j) in the k-th subbands at the l-th decomposition level. The SF in NSCT domain is defined in (1). SF is measured by using slipping window of coefficients in subbands. It measures the whole activity in the window-based coefficients via the gradient energy in rows and columns. SF in each subbands are inputted to PCNN to motivate the neurons and generate pulse of neurons with (2). Then, firing times $T_{i,j}^{l,k}$ is calculated as (3).

$$S_{i,j}^{l,k} = \sum_{i \epsilon M, j \epsilon N} (I_{i,j}^{l,k} - I_{i-1,j}^{l,k})^2 + (I_{i,j}^{l,k} - I_{i,j-1}^{l,k})^2 \quad (1)$$

$$\begin{cases} F_{ij}^{l,k}(n) = S_{ij}^{l,k} \\ L_{ij}^{l,k}(n) = e^{-\alpha_L} L_{ij}^{l,k}(n-1) + V_L \sum_{pq} W_{ij,pq}^{l,k} Y_{ij,pq}^{l,k}(n-1) \\ U_{ij}^{l,k}(n) = F_{ij}^{l,k}(n) * (1 + \beta L_{ij}^{l,k}(n)) \\ \theta_{ij}^{l,k}(n) = e^{-\alpha_\theta} \theta_{ij}^{l,k}(n-1) + V_\theta Y_{ij}^{l,k}(n-1) \\ Y_{ij}^{l,k}(n) = \begin{cases} 1, & \text{if } U_{ij}^{l,k}(n) > \theta_{ij}^{l,k}(n) \\ 0, & \text{otherwise} \end{cases} \end{cases} \quad (2)$$

$$T_{i,j}^{l,k} = T_{i,j}^{l,k}(n-1) + Y_{i,j}^{l,k}(n) \quad (3)$$

In the mathematical model of PCNN in (2), the feeding input $F_{ij}^{l,k}$ is equal to the normalized SF $S_{i,j}^{l,k}$. The linking input $L_{ij}^{l,k}$ is equal to the sum of neurons firing times in linking range. $W_{ij,pq}$ is the synaptic gain strength and subscripts p and q are the size of linking range in PCNN. α_L is the decay constants. V_L and V_θ are the amplitude gain. β is the linking strength. $U_{ij}^{l,k}$ is total internal activity. $\theta_{ij}^{l,k}$ is the threshold. n denotes the iteration times. If $U_{ij}^{l,k}$ is larger than $\theta_{ij}^{l,k}$, then, the neuron will generate

a pulse $Y_{ij}^{l,k} = 1$, also called one firing time. In fact, the sum of $Y_{ij}^{l,k}$ in n iteration is often defined as (3), called firing times, to represent image information. Rather than $Y_{ij}^{l,k}(n)$, one often analyzes $T_{ij}^{l,k}(n)$, because neighboring coefficients with similar features representing similar firing times in a given iteration times.

2.2 Image fusion algorithm based on NSCT-SF-PCNN

The core reason why PCNN is used in image fusion lies in its global coupling and pulse synchronization of neurons. These biological characteristics make full use of the local information in images, but not single coefficient information in most popular MSD-based fusion algorithms. Although a regional firing characteristic of PCNN[17] is investigated in multi-focus image fusion, we still use the firing times as a determination to select NSCT coefficients.

The schematic diagram of the proposed NSCT-SF-PCNN algorithm is shown in Fig. 5 and implemented as

1) Decompose the source images into subbands via NSCT.

2) Measure the SF as (1) in slipping window of coefficients in subbands.

3) SF in each subbands are input to PCNN to motivate the neurons and generate pulse of neurons with (2). Then, firing times $T_{ij}^{l,k}(n)$ is calculated as (3).

4) Get the decision map $D_{ij}^{l,k}$ based on (4) and select the coefficients with (5), which means that coefficients with large firing times are selected as coefficients of the fused image. This is the fusion rule proposed in this paper.

$$D_{F,ij}^{l,k} = \begin{cases} 1, & \text{if } T_{1,ij}^{l,k}(n) \geq T_{2,ij}^{l,k}(n) \\ 0, & \text{if } T_{1,ij}^{l,k}(n) < T_{2,ij}^{l,k}(n) \end{cases} \quad (4)$$

$$x_{F,ij}^{l,k} = \begin{cases} x_{1,ij}^{l,k}, & \text{if } D_{ij}^{l,k}(n) = 1 \\ x_{2,ij}^{l,k}, & \text{if } D_{ij}^{l,k}(n) = 0 \end{cases} \quad (5)$$

where $x_{F,ij}^{l,k}$, $x_{1,ij}^{l,k}$, and $x_{2,ij}^{l,k}$ denote the coefficients of the fused image and two source images, respectively.

5) Use the selected-out coefficients in (5) to reconstruct the fused image via inverse NSCT.

3 Experimental results

In this section, we use NSCT-SF-PCNN to fuse the multi-focus images, infrared and visible images, and remote sensing images. Parameters of PCNN is set as $p \times q$, $\alpha_L = 0.06931$, $\alpha_\theta = 0.2$, $\beta = 0.2$, $V_L = 1.0$, $V_\theta = 20$,

$$W = \begin{bmatrix} 0.707 & 1 & 0.707 \\ 1 & 0 & 1 \\ 0.707 & 1 & 0.707 \end{bmatrix}, \text{ and the maximal iterative num-}$$
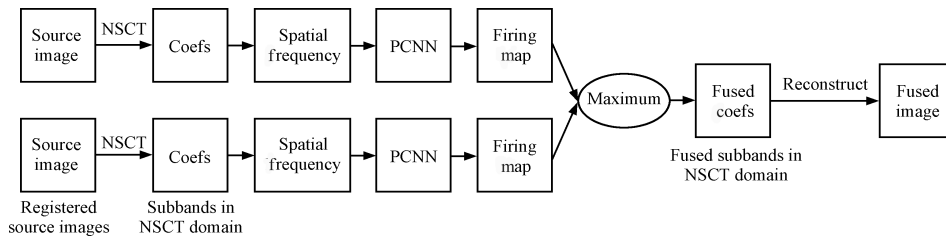
ber is $n = 200$.

Fig. 5 Schematic diagram of NSCT-SF-PCNN fusion algorithm

In order to show the advantages of the new algorithm, we establish three steps to demonstrate that the proposed NSCT-SF-PCNN outperforms other fusion algorithms. First, "db2" wavelet, atrous wavelet, contourlet, and NSCT are compared. Second, typical activity-level measurements in NSCT domain are compared. Third, typical PCNN-based fusion methods in wavelet, contourlet, and NSCT domain are compared. In the comparisons, besides visual observation, mutual information[19], and $Q^{AB/F}$[20] are used as information-based objective criteria. The reason is that image fusion aims at combining information and these criteria do not require the information of ideal fused image. Mutual information essentially computes how much information from source images is transferred to the fused image, whereas $Q^{AB/F}$ computes and measures the amount of edge information transferred from the source images to the fused images using a Sobel edge detector.

3.1 Comparisons on MSD methods

In this section, discrete wavelet transform (DWT) with basis "db2" and contourlet, which are shift-variant transforms, atrous wavelet transform, and NSCT,which are shift-invariant transforms, are compared. In these MSD methods, the average and maximum rules are used in the low-frequency and high-frequency domain, respectively.

Figs. 6 and 7 show the multifocus image fusion results and visible and infrared image fusion results of these methods. Focusing on the labeled region in Fig. 6, one can obviously find that the fused images of two shift-invariant methods, atrous wavelet and NSCT, are clearer and more natural than the DWT and contourlet fused results. It is proven that shift-invariant methods can overcome the pseudo-Gibbs phenomena successfully and improve the quality of the fused image around edges. In Fig. 7, the human presented with white color is being better extracted using contourlet and NSCT than that of DWT and atrous wavelet. Focusing on labeled region in Fig. 7, the house roof of the NSCT is clearer than that of other methods.

Furthermore, objective criteria on mutual information and $Q^{AB/F}$ in Table 1 indicate that NSCT method transferred more information to fused image than that of atrous wavelet, outperforming DWT and contourlet. So, it can be concluded that NSCT is the best MSD method. That is why NSCT is used as the MSD method in this paper.
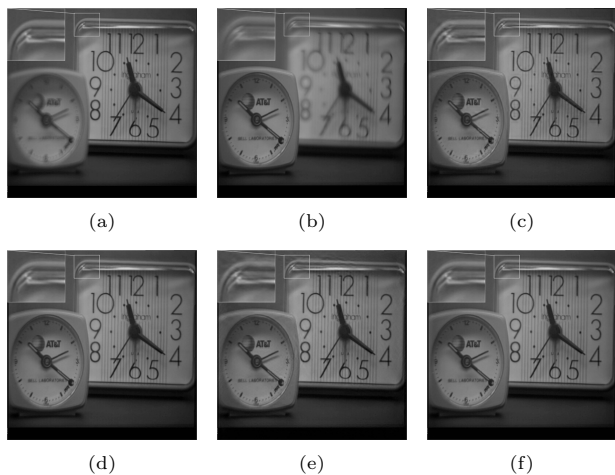
Fig. 6   Multifocus image fusion results of MSD-based algorithms ((a) clockA.tif: focus on right; (b) clockB.tif: focus on left; (c)∼(f) Fused images using DWT, atrous wavelet, Contourlet, NSCT)
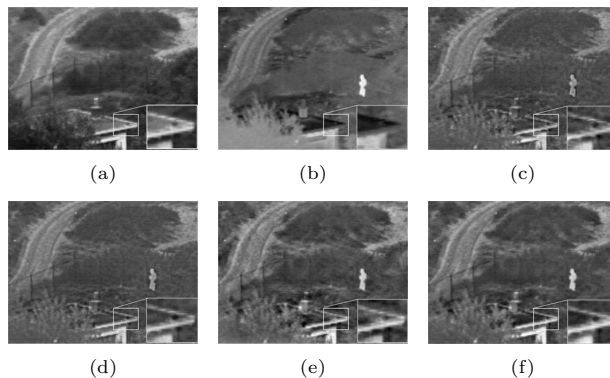
Fig. 7   Infrared and visible image fusion results of MSD-based algorithms ((a)Visible image: treesA.tif; (b) Infrared image: treesB.tif; (c)∼(f) Fused image using DWT, atrous wavelet, contourlet, NSCT)

Table 1   Comparison of objective criteria of different MSD methods

Images	Criteria	DWT	Atrous wavelet	Contourlet	NSCT
Clock	MI	6.3320	6.6208	6.0073	6.6761
	$Q^{AB/F}$	0.6099	0.6657	0.6122	0.6683
Tree	MI	1.4 719	1.5294	1.4822	1.5732
	$Q^{AB/F}$	0.4342	0.4674	0.4070	0.4828

3.2 Comparisons on activity-level measurement

In this section, all the comparisons are based on NSCT decomposition method. We compare the activity-level measurement of NSCT-SF-PCNN with other typical activity-level measurements in NSCT domain. In coefficients-max algorithms, absolute value of coefficients is used to measure the activity level directly. In SF-max algorithm, coefficients with greater SF in slipping window are considered in higher activity-level. Whereas in coefficient-PCNN and SF-PCNN algorithms, coefficients corresponding to greater firing times are considered in higher activity-level. All the coefficients with high activity-level are selected to compose the fused image[2].

Figs. 8 (c) ∼ (f) (see next page) show the high-frequency subimages and their SF in NSCT domain. Figs. 8 (g) ∼ (k) show the decision maps, in which the white color indicates that coefficients are selected from clockA.tif, otherwise selected from clockB.tif. Because the zoomed out part of clockA.tif shown in Fig. 8 (a) is clearer than in Fig. 8 (b), the optimal decision map would be in white color shown in Fig. 8 (k), which means all coefficients should be selected from clockA.tif. In Figs. 8 (e) and (f), it can be seen that SF extracts the edges of subimages well. Figs. 8 (g) and (i) indicate that SF considered as activity-level measurement is more reasonable than that from pure use of absolute value. Fig. 8 (h) shows that when the values of coefficients are input to motivate PCNN neurons, the global coupling and pulse synchronization of neurons benefits selecting coefficients, which considers the neighboring coefficients a lot. Thus, when SF is inputted to motivate PCNN neurons, one can imagine that NSCT-SF-PCNN could successfully accomplish the selection. The decision maps in Fig. 8 (j) show that the NSCT-SF-PCNN is the best one in the tested four activity-level measurements.

Listed in Table 2 is a comparison of the objective criteria of different activity-level measurements. The word coefficient is named coef for short, and coef-max means

the coefficients-max fusion rule. The greatest mutual information and $Q^{AB/F}$ demonstrate that the best activity-level measurement is successfully used in NSCT-SF-PCNN. However, in Fig. 10 the decision map of SF-max is better than PCNN, it is not consistent with Table 2, in which mutual information and $Q^{AB/F}$ of SF-max are smaller than that of PCNN. That is because we use PCNN in low-frequency subimage in coefficient-PCNN methods but we use average rule in SF-max methods.
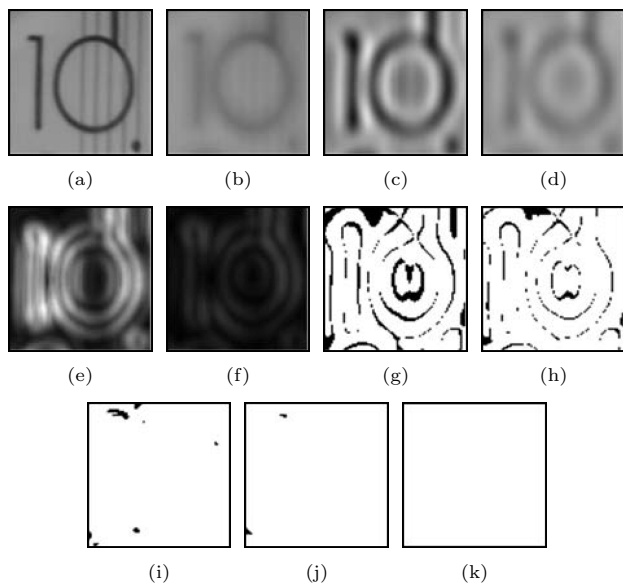

Fig. 8   SF of high-frequency subimages and the decision maps of typical activity-level measurements in NSCT domain ((a) Source image: zoomed out clockA.tif; (b) Source image: zoomed out clockB.tif; (c) ∼ (d) High-frequency subimages of (a) and (b) in NSCT domain; (e) ∼ (f) SF of (c) and (d); (g)∼(j) The decision maps of coefficients max rule, max rule on coefficient-PCNN, SF-max and maximum rule on SF-PCNN respectively; (k) Optimal decision map)

Table 2   Comparison of objective criteria of different activity level measurements in NSCT domain

Images	Criteria	Coef-max	SF-max	Coef-PCNN	SF-PCNN
Clock	MI	6.6761	6.8113	6.9559	7.4598
	$Q^{AB/F}$	0.6683	0.6735	0.6869	0.6880
Tree	MI	1.5732	1.5843	1.9670	2.1636
	$Q^{AB/F}$	0.4828	0.4896	0.5001	0.4972

3.3   Comparisons on typical PCNN-based algorithms

In this section, typical PCNN-based algorithms that are shift-invariant wavelet-PCNN (SIDWT-PCNN)[15], contourlet-PCNN[9] are compared with NSCT-SF-PCNN algorithms. The parameters of PCNN are set the same in the experiments.

Fig. 9 shows the multifocus image fusion results. NSCT-SF-PCNN and SIDWT-PCNN outperforms contourlet-PCNN in visual appearance because contourlet is shift-variant. Figs. 9 (a) and (c) show the difference between fused images, which are fused results using SIDWT-PCNN and NSCT-SF-PCNN, and source image in Fig. 6 (a). It indicates that NSCT-SF-PCNN extracts almost all the good-focalized part in source images and preserves the detailed information better than the SIDWT-PCNN.
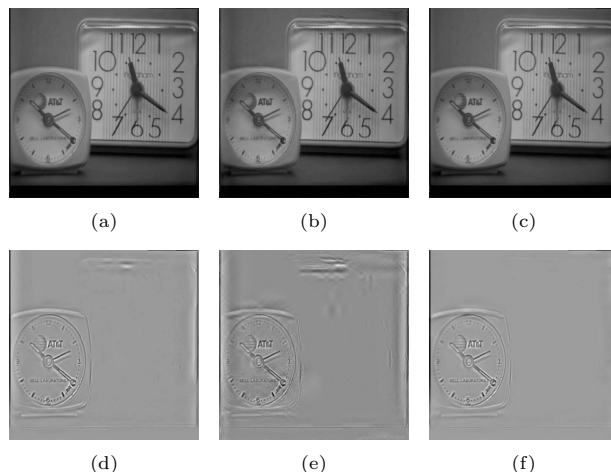

Fig. 9   Multifocus image fusion results ((a)∼(c) Fused images using SIDWT-PCNN, contourlet-PCNN and NSCT-SF-PCNN respectively; (d) Difference image between Fig. 9 (a) and Fig. 6 (a); (e) Difference image between Fig. 9 (b) and Fig. 6 (a); (f) Difference image between Fig. 9 (c) and Fig. 6 (a))

Fig. 10 shows the infrared and visible image fusion results. NSCT-SF-PCNN and contourlet-PCNN outperform SIDWT-PCNN in visual appearance. The result is consistent with that in [9], especially for infrared and visible image fusion, in which PCNN is used in contourlet domain. Figs. 10 (d) and (f) show the difference between fused images, which are fused results using contourlet-PCNN and NSCT-SF-PCNN, and source image in Fig. 7 (a). It indicates that NSCT-SF-PCNN extracts the trees better than contourlet-PCNN in visible image and human image being labeled with white color in infrared image.
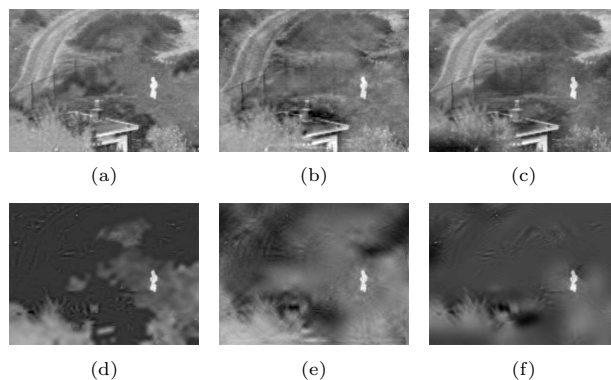

Fig. 10   Infrared and visible image fusion results ((a)∼(c) Fused images using SIDWT-PCNN, contourlet-PCNN and NSCT-SF-PCNN respectively; (d) Difference image between Fig. 10 (a) and Fig. 7 (a); (e) Difference image between Fig. 10 (b) and Fig. 7 (a); (f) Difference image between Fig. 10 (c) and Fig. 7 (a))

In Table 3 (see next page), all the objective criteria prove that fused image of the NSCT-SF-PCNN is strongly correlated with the source images and more image features, i.e., edges, are preserved in the fusion process, suggesting that the proposed NSCT-SF-PCNN is the best one in the three algorithms. Although in infrared and visible image fusion, mutual information of SIDWT is larger than that of NSCT-SF-PCNN, the visual appearance of SIDWT-PCNN fused image is not obviously good because the fused image of SIDWT-PCNN retains little information of visible image

in Fig. 7 (a). When all is said and done, our proposed algorithm outperforms other typical PCNN-based algorithms, whether in visual observation or objective evaluation criterion.

Table 3　Comparison of objective criteria of PCNN-based algorithms

Images	Criteria	SIDWT-PCNN	Contourlet-PCNN	NSCT-SF-PCNN
Clock	MI	6.9105	6. 0527	7.4598
	$Q^{AB/F}$	0.6834	0.6363	0.6880
Tree	MI	2.5714	1.4840	2.1636
	$Q^{AB/F}$	0.4732	0.3893	0.4972

3.4　Numerical experimental results

In order to demonstrate our NSCT-SF-PCNN is promising for the two applications, six group images in Fig. 11 are fused using methods of DWT[2], SIDWT-PCNN[15], and Contourlet-PCNN[9], CT-PCNN for short in Table 4. Because of the limited length of paper, only comparisons of objective criteria are given in Table 4. It is shown that NSCT-SF-PCNN is the best fusion algorithm with the greatest mutual information and $Q^{AB/F}$ in multifocus image fusion. In contrast, though the mutual information of NSCT-SF-PCNN is lower than that of SIDWT-PCNN when Figs. 11 (d) and (f) are fused, the $Q^{AB/F}$ of NSCT-SF-PCNN is larger than that of SIDWT-PCNN, and NSCT-SF-PCNN preserves visible feature better than SIDWT-PCNN as shown in Fig. 12.
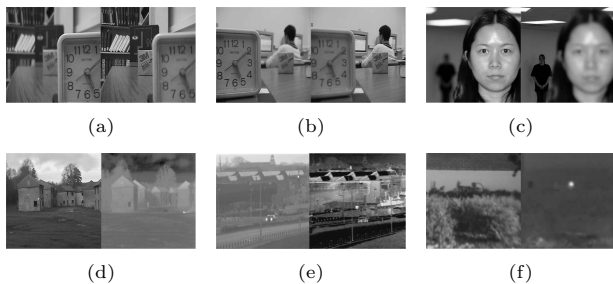

Fig. 11　Test images ((a)∼(c) Multifocus images;
(d)∼(f) Visible and infrared images)

Table 4　Comparison of objective criteria of PCNN-based algorithms

| Images (Fig. 11)	Criteria	DWT-max	SIDWT-PCNN	CT-PCNN	NSCT-SF-PCNN
(a)	MI	5.3948	5.9439	5.2640	6.2315
	$Q^{AB/F}$	0.6429	0.6839	0.6103	0.6885
(b)	MI	6.5199	7.3359	6.5603	7.5447
	$Q^{AB/F}$	0.6861	0.7216	0.6650	0.7 232
(c)	MI	5.7479	6.6863	6.2849	7.2704
	$Q^{AB/F}$	0.5681	0.6259	0.5652	0.6 273
(d)	MI	2.4257	4.0846	2.7957	3.6596
	$Q^{AB/F}$	0.5150	0.5736	0.5317	0.5859
(e)	MI	2.0367	2.5157	1.5856	3.0161
	$Q^{AB/F}$	0.6366	0.5817	0.5145	0.6666
(f)	MI	2.3481	5.6876	4.7955	5.6014
	$Q^{AB/F}$	0.6854	0.7998	0.7918	0.8 141
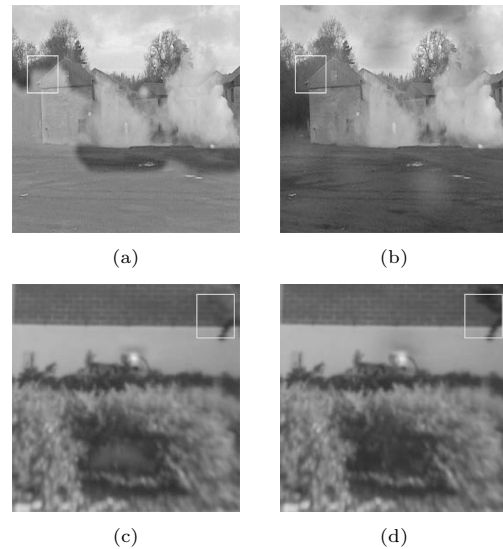
Fig. 12　Fused results of infrared and visible images ((a)∼(b)
The fused results of Fig. 11 (d); (c)∼(d) The fused results of
Fig. 11 (f) using SIDWT-PCNN and NSCT-SF-PCNN,
respectively)

4　Conclusion

In this paper, a spatial frequency motivated PCNN in NSCT domain, NSCT-SF-PCNN, is proposed. The flexible multiresolution, anisotropy, and directional expansion for images of NSCT are associated with global coupling and pulse synchronization characteristic of PCNN. Furthermore, a spatial frequency motivated PCNN, rather than pure use of coefficients value in traditional PCNN in image processing, is presented. Experiments on MSD methods, activity-level measurements, and typical PCNN-based algorithms demonstrate that the proposed NSCT-SF-PCNN is successful in multifocus image fusion and visible and infrared image fusion.

Acknowledgements

References

1　Hall D L, Llinas J. An introduction to multisensor data fusion. *Proceedings of the IEEE*, 1997, **85**(1): 6−23

2　Zhang Z, Blum R S. A categorization of multiscale-decomposition-based image fusion schemes with a performance study for a digital camera application. *Proceedings of the IEEE*, 1999, **87**(8): 1315−1326

3　Le P E, Mallat S. Sparse geometric image representation with bandelets. *IEEE Transactions on Image Processing*, 2005, **14**(4): 423−438

4　Do M N, Vetterli M. The contourlet transform: an efficient directional multiresolution image representation. *IEEE Transactions on Image Processing*, 2005, **14**(12): 2091−2106

5　Qu X B, Yan J W, Xie G F, Zhu Z Q, Chen B G. A novel image fusion algorithm based on bandelet transform. *Chinese Optics Letters*, 2007, **5**(10): 569−572

6　Choi M, Kim R Y, Nam M R, Kim H O. Fusion of multispectral and panchromatic satellite images using the curvelet

transform. *IEEE Geoscience and Remote Sensing Letters*, 2005, **2**(2): 136−140

7 Qu X B, Xie G F, Yan J W, Zhu Z Q, Chen B G. Image fusion algorithm based on neighbors and cousins information in nonsubsampled contourlet transform domain. In: Proceedings of International Conference on Wavelet Analysis and Pattern Recognition. Beijing, China: IEEE, 2007. 1797−1802

8 Zheng Yong-An, Song Jian-She, Zhou Wen-Ming, Wang Rui-Hua. False color fusion for multi-band SAR images based on contourlet transform. *Acta Automatica Sinica*, 2007, **33**(4): 337−341

9 Fang Yong, Liu Sheng-Peng. Infared Image Fusion Algorithm Based on Contourlet Transform and Improved Pulse Coupled Neural Networks, China Patent 1873693A, December 2006 (in Chinese)

10 Da Cunha A L, Zhou J P, Do M N. The nonsubsampled contourlet transform: theory, design, and applications. *IEEE Transactions on Image Processing*, 2006, **15**(10): 3089−3101

11 Eckhorn R, Reitboeck H J, Arndt M, Dicke P. Feature linking via synchronization among distributed assemblies: simulations of results from cat visual cortex. *Neural Computation*, 1990, **2**(3): 293−307

12 Johnson J L, Padgett M L. PCNN models and applications. *IEEE Transactions on Neural Networks*, 1999, **10**(3): 480−498

13 Broussard R P, Rogers S K, Oxley M E, Tarr G L. Physiologically motivated image fusion for object detection using a pulse coupled neural network. *IEEE Transactions on Neural Networks*, 1999, **10**(3): 554−563

14 Li M, Cai W, Tan Z. Pulse coupled neural network based image fusion. In: Proceedings of the 2nd International Symposium on Neural Networks. Chongqing, China: Springer, 2005. 741−746

15 Li W, Zhu X F. A new algorithm of multi-modality medical image fusion based on pulse-coupled neural networks. In: Proceedings of International Conference on Advances in Natural Computation. Changsha, China: Springer, 2005. 995−1001

16 Xu B C, Chen Z. A multisensor image fusion algorithm based on PCNN. In: Proceeding of the 5th World Congress on Intelligent Control and Automation. Hangzhou, China: IEEE, 2004. 3679−3682

17 Qu Xiao-Bo, Yan Jing-Wen, Zhu Zi-Qian, Chen Ben-Gang. Multi-focus image fusion algorithm based on regional firing characteristic of pulse coupled neural networks. In: Proceedings of International Conference on Bio-Inspired Computing: Theories and Applications. Zhengzhou, China: Publishing House of Electronics Industry, 2007. 563−565

18 Eskicioglu A M, Fisher P S. Image quality measures and their performance. *IEEE Transactions on Communications*, 1995, **43**(12): 2959−2965

19 Qu G H, Zhang D L, Yan P F. Information measure for performance of image fusion. *Electronics Letters*, 2002, **38**(7): 313−315

20 Petrovic V, Xydeas C. On the effects of sensor noise in pixel-level image fusion performance. In: Proceedings of the 3rd International Conference on Image Fusion. Paris, France: IEEE, 2000. 14−19
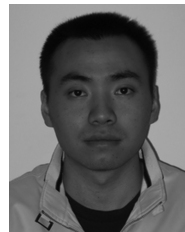
QU Xiao-Bo   Master student in the Department of Communication Engineering in Xiamen University. He received his bachelor degree from Xiamen University in 2006. His research interest covers image fusion, pulse coupled neural networks, wavelet and its applications, and new multiscale decomposition methods on images. E-mail: qxb_xmu@yahoo.com.cn
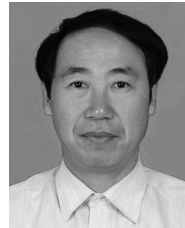
YAN Jing-Wen   Professor in the Department of Electronic Engineering, Shantou University. He received his Ph. D. degree in the State Key Laboratory of Applied Optics, Changchun Institute of Fine Mechanics Optics in Academia Sinica in 1997. He was approved as professor at Xiamen University in 2003. His research interest covers image compression, wavelet transform theory and its applications, and new multiscale decomposition methods on images. Corresponding author of this paper. E-mail: jwyan@stu.edu.cn

XIAO Hong-Zhi   Master student in the Department of Electronic Engineering, Shantou University. He received his bachelor degree from Shantou University in 2006. His research interest covers image and video compression, wavelet, and new multiscale transforms for images. E-mail: s_hzxiao@stu.edu.cn

ZHU Zi-Qian   Researcher at the Research Institute of Chinese Radar Electronic Equipment. He received his bachelor and master degree from Northwestern Polytechnical University in 1982 and 1989, respectively. His research interest covers multi-sensor data fusion, multi-object detection, and tracking in radar system. E-mail: zhuziqian@raa.org.cn